Chemical Engineering Journal 402 (2020) 126117

Contents lists available at ScienceDirect

Chemical Engineering Journal

journal homepage: www.elsevier.com/locate/cej

Nitrogen-doped reduced graphene oxide – PVDF nanocomposite membrane for persulfate activation and degradation of water organic micropollutants

Octávia Vieira, Rui S. Ribeiro*, Marta Pedrosa, Ana R. Lado Ribeiro, Adrián M.T. Silva

Laboratory of Separation and Reaction Engineering – Laboratory of Catalysis and Materials (LSRE-LCM), Faculdade de Engenharia, Universidade do Porto, Rua Dr. Roberto Frias, 4200-465 Porto, Portugal

HIGHLIGHTS

- N-doped reduced graphene oxide was synthesized using melamine (M) as N source (rGO-M).
- A rGO-M-PVDF composite membrane was prepared by including rGO-M in a PVDF matrix.
- rGO-M-PVDF promoted the activation of persulfate in continuous mode.
- Conversions of micropollutants in the range 54–91% were obtained.
- rGO-M-PVDF showed resistance towards fouling phenomena.

GRAPHICAL ABSTRACT

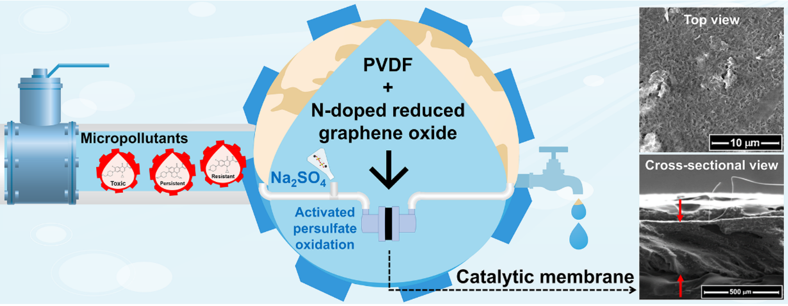

ARTICLE INFO

Keywords:
Carbon composite membrane
Metal-free catalyst
Persulfate oxidation
Continuous operation
Contaminants of emerging concern (CEC)

ABSTRACT

Metal-free carbon-based polymer nanocomposite membranes were employed for the first time for activated persulfate oxidation in continuous mode of operation. For that purpose, reduced graphene oxide doped with nitrogen by using melamine as source (rGO-M) was included as catalytic active phase in a poly(vinylidene fluoride) matrix (PVDF). The performance of the resulting composite membrane (rGO-M-PVDF) was compared against that obtained with supported membranes prepared by simple filtration of rGO-M into a PTFE substrate. The uniform distribution of rGO-M within both the surface pores and cross-sectional channels of the composite rGO-M-PVDF membrane (with a thickness of 292 ± 20 μm) was confirmed by scanning electron microscopy (SEM) and transmission electron microscopy (TEM), while its main structural features were studied by X-ray diffraction (XRD) and Raman spectroscopy. The quite good performance of this composite membrane was demonstrated by the degradation of three fluoroquinolone antibiotics at ppb level in ultrapure water (100 μg L^{-1} each), leading to average pollutant mass removal rates in the range 2.05–2.73 mg m^{-2} h^{-1}. Conversions of the pharmaceuticals in the range 54–91% were obtained even after 24 h of operation in full continuous mode. Persulfate conversion was confirmed and high resistance to fouling was observed with this novel catalytic membrane. Average pollutant mass removal rates in the range 0.34–0.77 mg m^{-2} h^{-1} were obtained in preliminary experiments performed with surface water instead of ultrapure water, highlighting the need for additional studies on both water matrix effects and process optimization.

---

* Corresponding author.
E-mail address: rsribeiro@fe.up.pt (R.S. Ribeiro).

https://doi.org/10.1016/j.cej.2020.126117
Received 21 March 2020; Received in revised form 23 June 2020; Accepted 27 June 2020

1. Introduction

Organic micropollutants – MPs (e.g., pesticides, synthetic and natural hormones, industrial compounds, pharmaceuticals and personal care products, among others) are typically released to the aquatic environment at trace concentrations (from ng L^{-1} to μg L^{-1}) [1]. Both conventional urban wastewater and drinking water treatment plants are not specifically designed to eliminate such compounds, many being resistant to biodegradation and persisting in the environment for long periods [2–4]. Some treatment technologies have been applied to address this issue, such as ozonation, adsorption on activated carbon and filtration [5]. In particular, processes based on sulfate radicals ($SO_4^{\bullet -}$) have recently gained a huge attention from the scientific community to tackle this issue [3]. Peroxymonosulfate and persulfate can be both activated by different approaches to generate $SO_4^{\bullet -}$ radicals (e.g., thermal, alkaline, or radiation methods, or employing metal or nonmetal catalysts) [6]. $SO_4^{\bullet -}$ possess similar or even higher reduction potential (between + 2.5 and + 3.1 V, depending on the activation method) than other radicals (such as hydroxyl radicals ($HO^{\bullet}$), chlorine radicals, superoxide radicals, carbonate radicals and perhydroxyl radicals), thus being able to oxidize most of the organic compounds in aqueous phase [3]. The whole process is known as activated persulfate oxidation.

Several metal-free materials (e.g., carbon materials, layered silicates and zeolites) emerged as promising alternatives to metal catalysts, avoiding traditional secondary contamination of the treated waters by leached metals [7–9]. Nevertheless, carbon materials typically have other advantages, such as large specific surface area, stability in acidic/basic media, the possibility to tailor the surface chemistry to improve the catalytic performance, and structural stability at high temperatures [10–12]. The main mechanism for the activation of the persulfate anion ($S_2O_8{}^{2-}$) by carbonaceous materials is based on an one-electron transfer, through the reaction described by Eq. (1) [3,8], but $HO^{\bullet}$ can also be formed through the reaction described by Eq. (2) [3,8]. In both cases, the radicals are the responsible species for the oxidation of the organic compounds [3]. Non-radical pathways can also occur, involving electron transfer from the organic pollutant to persulfate, and/or the generation of singlet oxygen ($^1O_2$) [3,8].

$$S_2O_8^{2-} + e^- \rightarrow SO_4^{-} + SO_4^{2-} \tag{1}$$

$$SO_4^{-} + OH^- \rightarrow SO_4^{2-} + HO^{\cdot} \tag{2}$$

Nanostructured carbon materials in powder form have been extensively employed in activated persulfate oxidation carried out in batch mode of operation [7,8]. However, only three studies have employed this type of materials in the form of membranes, a strategy that allows overcoming the constraints usually associated to the use of suspended powder catalysts and thus enabling operation in continuous mode [13,14]. The study performed by Liu et al. in 2016 [13] was the first report on this topic. Specifically, a metal-free N-doped reduced graphene oxide (N-rGO) catalyst was prepared by hydrothermal treatment of commercial graphene oxide (GO) with ammonia, and shaped as a catalytic membrane by simple vacuum filtration onto a PTFE substrate. The resulting carbon-supported membrane was then employed by the authors for sodium persulfate (SPS) activation and degradation of phenol (47 mg L^{-1}) in experiments performed in continuous mode during 3 h [13]. The second work on this topic was recently reported by our group [14]. In that study, graphite oxide was prepared and subjected to thermal treatment with different nitrogen precursors (melamine, urea and gaseous ammonia) in order to obtain N-rGO catalysts with different nitrogen contents. Moreover, a similar procedure was employed in the absence of nitrogen precursor to obtain undoped rGO. The material prepared with melamine (rGO-M) yielded the highest catalytic activity. This superior performance was ascribed to the presence of nitrogen-rich active sites, in particular to N-pyridinic groups. rGO-M was shaped as a catalytic membrane through the vacuum filtration methodology using PTFE as support, and employed for SPS activation and degradation of both phenol (5 mg L^{-1}) and oxalic acid (30 and 90 mg L^{-1}) in experiments performed in continuous mode during 6.5 h [14]. In the third study – and so far the last reported on this topic, rGO was assembled with multi-walled carbon nanotubes, shaped as a membrane upon vacuum filtration into a nylon substrate, and employed for SPS activation and degradation of sulfamethoxazole (500 μg L^{-1}) in experiments performed in continuous mode during 3 h [15]. In all these three previous studies, the catalytic active phase was placed on the top of a certain support (PTFE or nylon). However, these membranes can suffer partial disintegration upon continuous operation, drying and/or reuse.

The main goal of the present study is to optimize membrane design, in order to obtain more robust metal-free carbon-based membranes for SPS activation and degradation of water organic MPs in continuous mode of operation. For that purpose, carbon – polymer nanocomposite membranes were prepared instead. Poly(vinylidene fluoride) (PVDF) was selected as polymeric matrix since PVDF membranes often present high chemical resistance, thermal stability, inertness and good mechanical properties [16], and rGO-M (prepared as described in our previous work [14]) was incorporated as catalytic active phase in the membrane forming materials. The resulting composite membrane (rGO-M-PVDF) was characterized by thermogravimetric analysis (TGA), water contact-angle measurements, scanning electron microscopy (SEM), transmission electron microscopy (TEM), X-ray diffraction (XRD), and Raman spectroscopy. The performance of rGO-M-PVDF in activated persulfate oxidation was then evaluated using aqueous solutions containing three target MPs (100 μg L^{-1} each). The MPs selected in this study are three fluoroquinolone antibiotics, namely ofloxacin (OFX), ciprofloxacin (CIP) and enrofloxacin (EFX), which are briefly characterized in Table S1. EFX is used in veterinary practice and was one of the MPs detected at higher concentration in a recent study of our group on the occurrence of MPs in Portuguese surface waters [17], whereas OFX and CIP are used in human medicine and have also been found in several environmental samples [4]. CIP was recently included in the Watch List of contaminants of emerging concern for which additional monitoring/impact studies are required as defined in the Commission Decision 2018/840/EU [18]. Moreover, surface water (SW; cf. Section 2.2) was used in addition to studies with ultrapure (UP) water, in order to achieve conditions closer to a real case study. The results herein obtained were compared with those previously reported in the literature on both metal containing and metal-free carbon-based membranes for activated persulfate oxidation.

2. Materials and methods

2.1. Reagents

Synthetic graphite (particle size < 20 μm; catalogue number 282863), melamine (99 wt%), polyvinylpyrrolidone (PVP; MW: 40,000 g mol^{-1}), 1-methyl-2-pyrrolidone (NMP; 99.5 wt%), poly(vinylidene fluoride) (PVDF; MW: 275,000 g mol^{-1}), ciprofloxacin hydrochloride (European Pharmacopoeia reference standard), and enrofloxacin (98 wt%) were purchased from Sigma-Aldrich. Sulphuric acid (H_2SO_4; 95 wt%), ofloxacin (98 wt%), disodium hydrogen phosphate (Na_2HPO_4; 99 wt%), monosodium phosphate (NaH_2PO_4; 99 wt%), and N, N-Dietyl-p-plenylenediamine sulfate (DPD; 99 wt%) were obtained from Fluka. Sodium nitrate ($NaNO_3$; 99 wt%), formic acid (99 wt%), potassium permanganate ($KMnO_4$; 99.5 wt%), and absolute ethanol were obtained from VWR. Hydrogen peroxide (H_2O_2; 30 wt%) and methanol (HPLC grade) were supplied by Panreac and Fisher, respectively. Sodium persulfate (SPS; MW: 238.110 g mol^{-1}, 99 wt%) was supplied by Riedel-de Haën. All chemicals were used as received, without further purification. Ultrapure water was produced in a Milli-Q® water purification system (Merck, Darmstadt, Germany).

2.2. Water matrices

Solutions containing the three MPs under study were prepared in (i) ultrapure water (UP; pH = 5.9) and (ii) surface water (SW; pH = 7.4; 4.0 mg L^{-1} dissolved organic carbon; 120 mg L^{-1} total dissolved solids; 13.3 mg L^{-1} chlorides; 3.6 mg L^{-1} nitrates; 22.5 mg L^{-1} sulphates; < 0.05 mg L^{-1} phosphates; 11.1 mg L^{-1} sodium; 25.2 mg L^{-1} calcium; 5.1 mg L^{-1} magnesium) collected nearby the admission point of a drinking water treatment plant located in the district of Porto, Portugal. SW was filtered (2 µm glass fiber filters; Filtres RS, Paris, France) prior to its use in this work, in order to eliminate suspended solids that would interfere in subsequent analytical steps, and kept at 4 °C until further use.

2.3. Synthesis of graphene derivatives

2.3.1. Graphite oxide

Graphite oxide was prepared by a modified Hummers' method, as described elsewhere [19]. For that purpose, 240 mL of concentrated H_2SO_4 was added gradually under stirring (300 rpm) to a 2 L glass beaker containing 5 g of graphite and immersed in an ice bath to avoid overheating. Then, 5 g of $NaNO_3$ was slowly added to the mixture, followed by adding 30 g of $KMnO_4$. The mixture was stirred for 5 to 10 min prior to the addition of each reagent. In the next step, the mixture was removed from the ice bath and placed in an oil bath at 35 °C under stirring (300 rpm) for 12 h. After that period, the mixture was cooled down in an ice bath under stirring (400 rpm), diluted with 1250 mL of distilled water, and 35 mL of H_2O_2 (30 wt%) was added. The mixture was then centrifuged during 30 min at 3000 rpm, to remove the excess of acid. The resulting paste was filtered, washed with distilled water until reaching pH 5 in the rinsing waters, and dried overnight at 60 °C to obtain graphite oxide.

2.3.2. N-doped reduced graphene oxide (rGO-M)

Nitrogen-doped reduced graphene oxide (rGO-M) was obtained by pyrolysis of graphite oxide in the presence of melamine (M), using a modified procedure described elsewhere [20]. For that, 0.5 g of graphite oxide and 0.4 g of M were added to 30 mL of absolute ethanol. After kept in an ultrasonic bath for 30 min, the mixture was distributed into two crucibles and dried at 60 °C. The resulting material was then subjected to thermal treatment at 350 °C for 30 min in a muffle furnace under static air (Nabertherm P330, Lilienthal, Germany), with a heating rate of 5 °C min^{-1}. Once cooled down to room temperature, the obtained black powder was washed with 1 L of distilled water under vacuum filtration and dried overnight at 60 °C, resulting in the rGO-M materials.

2.3.3. rGO-M-PVDF membranes

Composite polymeric membranes were fabricated considering 6.4 wt% of rGO-M in the membrane forming materials, by modifying a procedure previously described elsewhere [21]. For that purpose, 0.464 g of rGO-M was added to a solution containing 0.070 g of PVP in 6.0 mL of NMP, the resulting mixture being sonicated for 3 h at room temperature. 1.07 g of PVDF was then added to the mixture, and the polymerization proceeded at 40 °C for 48 h, using an oil bath. Afterwards, the polymer solution was left unstirred overnight at room temperature to allow air bubbles to escape. The polymer solution was then placed in a glass plate and spread using the knife cast technique (cf. Fig. 1). The casting knife film applicator (Elcometer 3580, Warren, MI) allows selecting the thickness of the cast polymer solution (50 µm), which was then immersed in distilled water; after complete coagulation, a flat membrane sheet of rGO-M-PVDF was removed from the glass plate, cut to 1.64 cm of inner diameter (2.10 cm^2 of effective area), and stored in distilled water until further use. The dry weight of each resulting rGO-M-PVDF membrane was 23 mg. Considering that the fraction of rGO-M in the membrane forming materials is 6.4 wt%, it is assumed that the mass of rGO-M in the composite membrane is ca. 1.5 mg. For characterization purposes, a PVDF membrane was prepared as described, but without adding rGO-M.

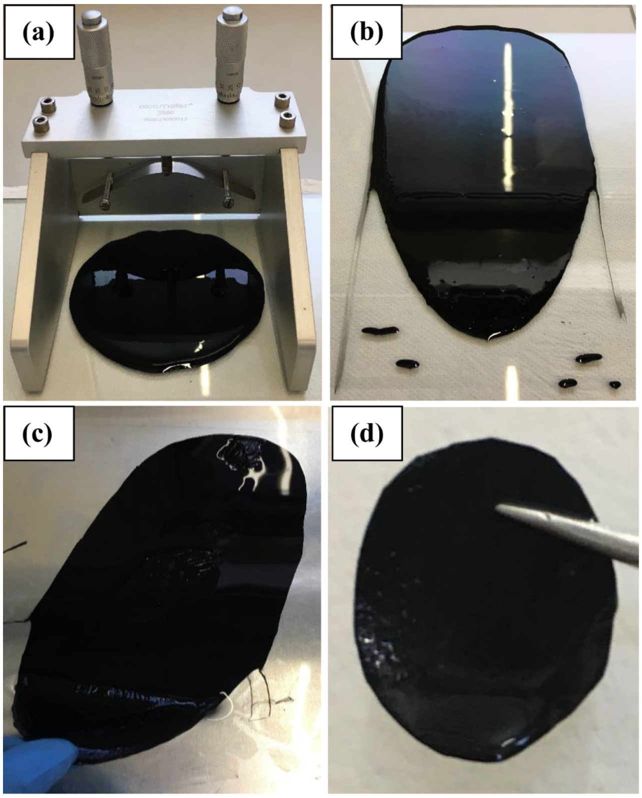

Fig. 1. Application of the knife cast technique: (a) placement of the polymer solution in a glass plate, which was then (b) spread using the casting knife shown in (a); (c) flat membrane sheet obtained after complete coagulation of the solution; and (d) rGO-M-PVDF membrane with the desired dimensions.

2.3.4. rGO-M supported membranes

Supported membranes were manufactured by simple vacuum filtration of a rGO-M dispersion, as described elsewhere [14]. For that purpose, 15 mg of rGO-M was dispersed in 30 mL of NMP, homogenized in an ultrasonic bath for 1 h, and then vacuum filtered into a Millipore JGWP PTFE substrate (0.2 µm pore size; 1.64 cm of inner diameter; 2.10 cm^2 of effective area). The resulting membrane was washed with distilled water prior to application.

2.4. Characterization techniques

Thermogravimetric analysis (TGA) was performed in a Netzsch STA 490 PC/4/H Luxx thermal analyser, in which the sample was heated in an air flow from 50 to 900 °C at 20 °C min^{-1}.

Temperature programmed desorption (TPD) was performed in a fully automated AMI-300 Catalyst Characterization Instrument (Altamira Instruments, Pittsburgh, PA), equipped with a quadrupole mass spectrometer (Dymaxion, Ametek, Pittsburgh, PA), as described elsewhere [22]. The concentration of CO_2 and CO were obtained by integrating the area of the respective spectra. Deconvolution analysis of the CO_2 and CO TPD spectra was performed using a well-established procedure [22,23]. Accordingly, the peaks in the CO_2 TPD spectra were assigned to different functional groups, namely: carboxylic acids (CA), carboxylic anhydrides (CAn), and lactones (Lac). Likewise, the peaks in the CO TPD spectra were assigned to: carboxylic anhydrides (Can), phenols (Ph), carbonyls and quinones (CQ), and basic surface groups (Bas), such as pyrones and chromenes. In the CO_2 spectra, the width at half-height (*W*) was considered the same for Can and Lac; in the CO spectra, the same *W* was considered for Ph and CQ whenever peak shoulders were unclear.

The hydrophobicity/hydrophilicity of the metal-free carbon membranes was estimated by static water contact-angle measurements through the sessile-drop method [24], using an Attention optical tensiometer (model Theta) for image acquisition and data analysis. Measurements were performed on dry membranes, the contact-angle being obtained from triplicate measurements performed in different locations of each sample.

Scanning electron microscopy (SEM) images were obtained using a FEI Quanta 400 FEG ESEM/EDAX Genesis X4M instrument equipped with an Energy Dispersive Spectrometer (EDS). The clean cut required to perform cross-sectional characterization was performed under cryogenic conditions, by immersing the polymeric membranes in liquid nitrogen. Twenty measurements were performed by using ImageJ software in order to estimate the average thickness of the rGO-M-PVDF membranes.

X-ray diffraction (XRD) analysis was performed in a PANalytical X'Pert PRO diffractometer set at 45 kV and 40 mA, and equipped with a PIXcell detector (CuKα = 0.1542 nm; data recorded at a 0.01° step size). Interplanar spacing (*d*-spacing) was calculated by using Bragg's law.

Raman spectra were recorded at ambient temperature with a 100 × Zeiss EC Epiplan air objective (numerical aperture of 0.9), using a confocal Raman system (Alpha 300R, Witec) with a 532 nm laser excitation. Raman spectra of rGO-M powder and rGO-M-PVDF membrane was taken with 600 g mm^{-1} diffraction grating, 0.5 mW laser power at the focal plane, 12 s integration time and 20 accumulated acquisitions, whereas the laser power was increased to 14 mW in the case of the PVDF membrane (to allow the Raman signal to be observed). The bright field reflective image of the rGO-M-PVDF nanocomposite membrane was obtained with the same 100 × objective. Raman mapping images were collected within a 5 × 5 µm region of the rGO-M-PVDF membrane, using a sum filter to add all the collected Raman shift intensity values within a 100 cm^{-1} bandwidth (which cover the D and G band peaks).

Transmission electron microscopy (TEM) images and electron diffraction patterns were collected using a JEOL 2100 instrument operating at 80 kV, equipped with a LaB_6 electron gun and a 4 k × 4 k CCD camera that operates at 25 fps (300 fps with 512 × 512 pixel) and features drift correction. Sectioning of the rGO-M-PVDF membrane with a dialled in thickness of 200 nm was performed by cryo-microtomy, using a Boeckeler PowerTome PC Ultramicrotome RMC, after immersing the polymeric membrane in liquid nitrogen. Forty four measurements were performed by using ImageJ software in order to estimate the average number of stacked graphene layers of rGO-M.

2.5. Activated persulfate experiments

Activated persulfate experiments were carried out at room temperature (22 ± 2 °C), using the experimental set-up shown in Fig. 2. The solution containing the MPs under study (100 µg L^{-1} each) and the selected amount of SPS (25 mg L^{-1}) was fed in continuous mode to the membrane cell (at a flow rate of 0.10 mL min^{-1}), the treated water being collected in a glass bottle. Pure adsorption tests were performed in the absence of SPS. A non-catalytic experiment was performed in batch mode, in order to evaluate the stability of the selected MPs in the presence of SPS. All the experiments were performed without pH adjustments, with the inherent pH of ultrapure water (pH = 5.9) or surface water (pH = 7.4).

2.6. Analytical methods

The concentrations of OFX, CIP and EFX were determined by ultra-high-performance liquid chromatography (UHPLC), using a Shimadzu Corporation apparatus (Tokyo, Japan) consisting of an autosampler (SIL-30AC), a degasser (DGU-20A5), an oven (CTO-20AC), two pumps (LC-30AD), a fluorescence detector (FD; RF-20AXS), and a system controller (CBM-20 A Lite). Chromatographic separation was optimized using a Kinetex™ 1.7 µm F5 100 Å column (100 × 2.1 mm i.d.) supplied by Phenomenex, Inc. (Torrance, CA), set at 40 °C. A mixture of (A) 0.1% aqueous formic acid and (B) methanol was used as mobile phase (total flow rate of 0.3 mL min^{-1}), delivered as follows: 25% of B for 0.5 min, a linear gradient from 25% to 65% during 9 min (kept during 0.5 min), a linear gradient from 65% to 25% in 0.5 min and finally an equilibration time of 7.5 min, corresponding to a total run time of 18 min. The autosampler temperature was kept at 15 °C, and the injection volume was 30 µL. The excitation wavelength of the FD was 290 nm and the emission wavelength was 460 nm. For quantification purposes, small aliquots were periodically withdrawn from the reactor and an excess of methanol was immediately added in order to stop the reaction, the samples being then refrigerated at 4 °C prior to analysis.

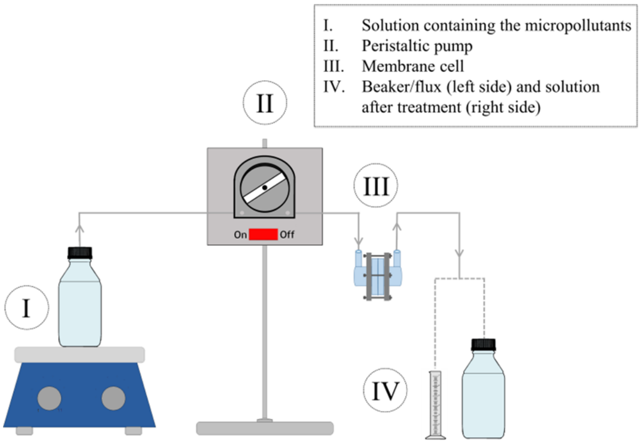

Fig. 2. Schematic representation of the experimental set-up used for the experiments.

The concentration of SPS was determined by a colorimetric method with N,N-Dietyl-p-plenylenediamine sulfate (DPD), by adapting the procedure reported elsewhere [25]. Firstly, two working solutions were prepared: (i) phosphate buffer (100 mmol L^{-1}, pH = 7, 50 mL), obtained by adding 0.4144 g of Na_2HPO_4 and 0.2569 g of NaH_2PO_4; and (ii) DPD solution (25 mmol L^{-1}, 10 mL), obtained by dissolving 0.0655 g of DPD in H_2SO_4 (0.05 mol L^{-1}). For stability purposes, the DPD solution was stored in an amber bottle at 4 °C for no more than one week. In each measurement, 500 µL of sample was added to 2.5 mL of phosphate buffer, and diluted with 1.5 mL of ultrapure water. 500 µL of the DPD solution was then added and the color developed during 10 min at room temperature. Absorbance was recorded at 551 nm (maximum absorbance peak) against a blank prepared by replacing the sample by ultrapure water, using a JASCO V-570 UV/VIS spectrophotometer (Easton, MD). The samples were withdrawn periodically, and immediately refrigerated at 4 °C prior to analysis.

The dissolved organic carbon and concentration of ions in SW were determined as previously described [26]. The content of total dissolved solids was determined from the dry residue obtained after drying at 180 °C until constant weight [27].

2.7. Permeation of the membranes

Water permeate flux (J_W) was monitored during the activated persulfate experiments, by application of Eq. (3) [28]. *V*, *S* and Δ*t* represent the volume of permeated water, effective area of the membrane, and permeation time, respectively.

2.8. Pollutant mass removal rate

The performance of the metal-free carbon-based membranes for SPS activation and degradation of water organic MPs was evaluated through an additional parameter, defined as pollutant mass removal rate (m_{Removal}) and obtained as described in Eq. (4). $[\mathrm{Pollutant}]_0$ and $[\mathrm{Pollutant}]_{\mathrm{Effluent}}$ represent the concentration of a given pollutant in the influent and effluent of the membrane cell, respectively.

$$J_{\mathrm{w}} = \frac{V}{S\Delta t} \tag{3}$$

$$m_{\mathrm{Removal}} = J_{\mathrm{w}} \times ([\mathrm{Pollutant}]_0 - [\mathrm{Pollutant}]_{\mathrm{Effluent}}) \tag{4}$$

3. Results and discussion

3.1. Characterization

rGO-M was characterized in our previous publication [14] by elemental analysis, Fourier-transform infrared spectroscopy (FTIR), X-ray diffraction (XRD), X-ray photoelectron spectroscopy (XPS), nitrogen adsorption-desorption isotherms, SEM and scanning transmission electron microscopy (STEM). Briefly, rGO-M is a nitrogen-rich (23.78 wt%) reduced GO material, the deconvolution of the N1s region obtained by XPS revealing 41.56, 38.07 and 20.37 at. % of N-pyrrolic (N5), N-pyridinic (N6) and N-quaternary (NQ) species, respectively (cf. Fig. S1). Complementary characterization data was obtained in the present study. In particular, the occurrence of oxygen-containing surface functionalities was investigated by TPD. As observed in Table 1 (data obtained from Fig. S2), graphite oxide possesses a high oxygen content (44.0 wt%). The procedure carried out for simultaneous reduction, exfoliation and N-doping of graphite oxide (cf. Section 2.2.2) was effective, as revealed by the lower oxygen content of rGO-M (6.3 wt%), which demonstrates that rGO-M is a partially reduced GO material.

Deconvolution analysis of the CO_2 and CO TPD spectra was performed in order to identify and quantify the amounts of the different functional groups present at the surface of rGO-M (cf. Fig. 3 and Tables S2 and S3). Surface groups were not released as CO_2 and CO for temperatures below 350 °C, i.e., the temperature at which rGO-M was thermally treated with melamine. Carboxylic acids (released as CO_2), phenols (released as CO) and carboxylic anhydrides (released as CO_2 and CO) were the main oxygen-containing surfaces groups identified.

Water contact-angle measurements were performed for both rGO-M (in the form of the PTFE supported membrane) and rGO-M-PVDF membrane. As expected, rGO-M is a highly hydrophilic material due to the high content of carboxylic acids (918 μmol g^{-1}). In this case, the water droplet is immediately spread on the surface, not allowing proper contact angle measurement. This is a common limitation of sessile-drop goniometry for small contact angles (below 20°) [24]. On the other hand, the water contact-angle obtained for the rGO-M-PVDF nanocomposite membrane was 69 ± 3° (cf. Fig. S3), revealing its less hydrophilic character.

TGA analysis under air atmosphere demonstrates the resistance of the rGO-M-PVDF nanocomposite membrane to temperatures up to 350 °C (cf. Fig. 4).

The properties and distribution of rGO-M within the rGO-M-PVDF composite membrane were studied by SEM, TEM, XRD and Raman spectroscopy. For that purpose, the rGO-M powder material and the PVDF membrane (prepared without adding rGO-M) were first characterized by SEM. Briefly, rGO-M has the typical morphology (cf. Fig. 5a) and elemental composition (cf. Fig. S4a) of N-doped reduced graphene oxide prepared from chemical oxidation of graphite by the Hummers' method [14]. The PVDF membrane possesses the typical surface pores and cross-sectional channels (cf. Fig. 5b and d) of polymeric membranes [16]. When these materials are combined in the fabrication of the rGO-M-PVDF composite membrane, rGO-M is effectively embedded in the polymeric matrix while the morphological features of the membrane remain the same (cf. Fig. 5c and e). Indeed, a uniform distribution of rGO-M is obtained within both the surface pores (cf. Fig. 5c) and cross-sectional channels (cf. Fig. 5e) of the composite membrane. The average thickness of the rGO-M-PVDF membranes is 292 ± 20 µm (as determined from SEM measurements). EDS analysis confirmed that the rGO-M-PVDF membrane is mainly composed of carbon, fluorine and oxygen (cf. Fig. S4b).

Table 1
Amounts of CO_2 and CO released by TPD, and corresponding percentage of oxygen (assuming that all the surface oxygen is released as CO_2 and/or CO).

Material	CO_2 (μmol g^{-1})	CO (μmol g^{-1})	O (wt.%)	CO/CO_2
Graphite oxide	11,629	4262	44.0	0.4
rGO-M	1389	1165	6.3	0.8

The crystalline structure of rGO-M, and PVDF and rGO-M-PVDF membranes was studied by XRD (cf. Fig. 6). The XRD pattern of the rGO-M powder reveals a broad peak (typical of multi-layer graphene reduced graphene oxide) centered at 26.5° (*d*-spacing of 0.336 nm), corresponding to the characteristic crystalline graphite (0 0 2) plane [29,30]. Indeed, the value of *d*-spacing found for rGO-M is near to that typically obtained for graphite (0.335 nm) [29,30], which confirms the absence of intercalated species between the graphene layers of rGO-M, and thus the effectiveness of the reduction treatment. Therefore, it can be concluded that most of the oxygen and nitrogen containing functionalities, as determined by TPD and XPS, respectively, are preferably located in the edge plane of the graphene sheets of rGO-M. The PVDF membrane is mainly composed by the α-phase, as evidenced by the two intensive diffraction peaks at 18.4 and 20.0°, and the smaller peak at 26.6°, which correspond to the characteristic (0 2 0), (1 1 0) and (0 2 1) reflections of the monoclinic α-phase crystal, respectively [31]. The XRD pattern of the rGO-M-PVDF composite membrane reveals that the crystalline properties of both rGO-M powder and PVDF membrane are negligibly affected when rGO-M is embedded in the polymeric matrix. Specifically, the graphite (0 0 2) plane shifts slightly, from 26.5° in the rGO-M powder, to 26.6° in the rGO-M-PVDF composite membrane, which corresponds to a *d*-spacing of 0.335 nm. These results show that the distance between the graphene layers does not increase, allowing to conclude that PVDF is not intercalated within the graphene layers of rGO-M during the fabrication of the rGO-M-PVDF composite membrane. This can be ascribed to the absence of intercalated species in the rGO-M lattice, as discussed previously. Therefore, XRD results confirm that rGO-M is distributed within the pores of the polymeric matrix.

The structure of rGO-M, and PVDF and rGO-M-PVDF membranes was studied by Raman spectroscopy. The Raman spectra of rGO-M reveals three peaks, corresponding to the D, G and 2D bands, observed at 1352, 1590 and 2818 cm^{-1}, respectively (cf. Fig. 7a). The G band corresponds to an E_{2g} mode of hexagonal graphite and the vibration of sp^2-hybridized carbon domain, whereas the D band is an indication of structural disorder [32]. Indeed, the intensity ratio of the D band relative to the G mode (I_D/I_G) is 2.04, corresponding to a disordered reduced graphene oxide structure. This may be a beneficial feature for activated persulfate oxidation, considering that enhanced catalytic performances have already been ascribed to the presence of structural defects in graphene sheets. One example is our previous publication on the application of reduced graphene oxide samples with different structural disorder in catalytic wet peroxide oxidation [33]. The presence of a broad 2D band is typical of multi-layer graphene-based materials [29], which is in agreement with XRD results. The Raman spectra of the PVDF membrane reveals several peaks, including the four characteristic peaks attributed to the α-phase, observed at 284, 535, 610, and 795 cm^{-1} (cf. Fig. 7b) [34]. These results suggest the prevalence of the α-phase, which is in agreement with the XRD analysis. However, one characteristic peak of the β-phase appears at 839 cm^{-1}, indicating that this phase is also present [34]. It should be noted that

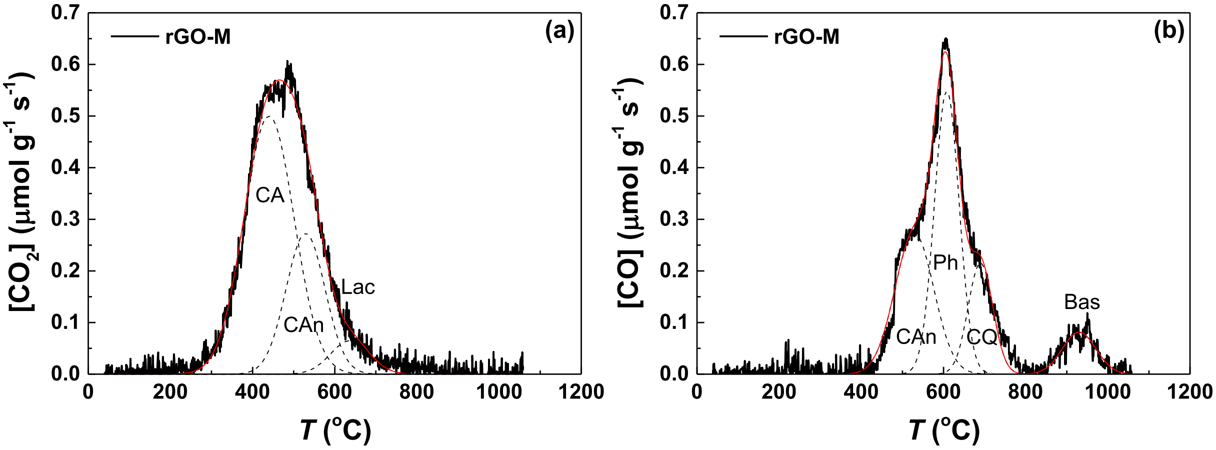

Fig. 3. Deconvolution results of (a) CO_2 and (b) CO TPD spectra of rGO-M. Dashed lines represent peaks assigned to carboxylic acids (CA), carboxylic anhydrides (Can), lactones (Lac), phenols (Ph), carbonyls and quinones (CQ) and basic surface groups (Bas), such as pyrones and chromenes. Red lines represent cumulative peak fitting. (For interpretation of the references to color in this figure legend, the reader is referred to the web version of this article.)

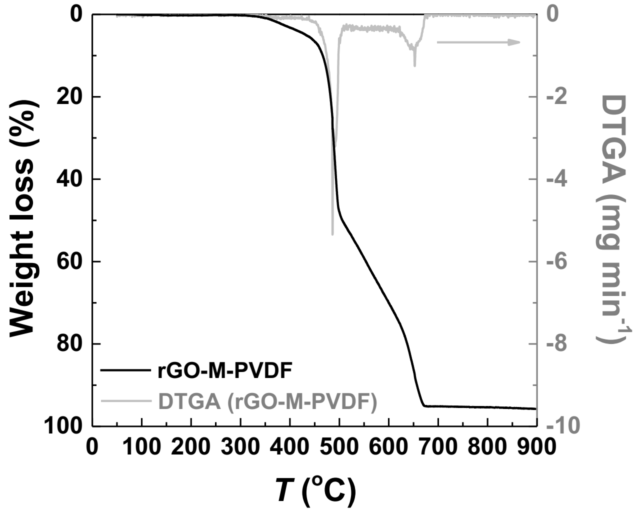

Fig. 4. Thermogravimetric analysis (TGA) of rGO-M-PVDF nanocomposite membrane in oxidative (air) atmosphere.

the Raman spectra of the PVDF membrane was taken with 14 mW laser power at the focal plane, while 0.5 mW was used for rGO-M and rGO-M-PVDF (in this case, to avoid thermal damage and allow direct comparison with rGO-M) characterization. This was needed due to the lower Raman signal yielded by PVDF. Therefore, the Raman spectra of the rGO-M-PVDF nanocomposite membrane only depicts the three peaks corresponding to the rGO-M powder (cf. Fig. 7a). As observed, no major structural changes occur. The I_D/I_G ratio increases slightly, from 2.04 to 2.19, indicating that some structural defects are induced in the graphene sheets of rGO-M during the fabrication of the composite membrane. The G band shifts slightly, from 1590 to 1594 cm^{-1}. Moreover, the bright field reflective image of rGO-M-PVDF reveals some granulation at the surface of the membrane (cf. Fig. S5a). Raman spectroscopic mapping was carried out to confirm the homogeneous structure of rGO-M when embedded in the PVDF matrix (cf. Fig. S5b and c). It should be noted that the darker regions in these images do not indicate the absence of rGO-M, they are just the result of smaller Raman signal in those regions, due to the porous/granulated character of the rGO-M-PVDF nanocomposite membrane. As observed in the composite image given in Fig. S5d, the structural order of rGO-M is nearly homogeneous, as only slight non-uniformities between the signals of the D and G bands (i.e., I_D/I_G ratio) are observed within the region under study. These are indicated by the faint red circles, which highlight regions with less defective graphene layers.

TEM was used to study the atomic structure and estimate the number of graphene layers in rGO-M (cf. Fig. 8a, b and c). The central part of graphene sheets is usually seen as a uniform and spotless area, although some wrinkles can be identified as dark marks and the sheets tend to roll near the edges [29]. In the case of rGO-M, these features are particularly clear in the TEM micrograph given in Fig. 8a. Each folded graphene sheet is locally parallel to the electron beam, exhibiting a dark line that can be used to estimate the number of graphene layers present in rGO-M by direct visualization [29], as shown in Fig. 8c. Based on 44 measurements performed within TEM micrographs taken in 5 different sampling areas, it was found that rGO-M consists of 5 to 12 stacked graphene layers, an average value of 8 ± 2 layers being estimated (cf. Fig. 8c). The electron diffraction pattern given in Fig. 8e also confirms the polycrystalline nature of rGO-M. Moreover, the diffraction rings are consistent with the (1 1 0) and (1 0 0) planes of graphite, and suggest that there is no preferred stacking orientation among the overlapping graphene layers [35]. All these observations confirm the multi-layer nature of rGO-M, as defined elsewhere [36]. Moreover, the *d*-spacing determined by XRD was confirmed through TEM measurements (cf. Fig. 8c). The rGO-M-PVDF membrane was also analysed by TEM. However, the thickness of the membrane (292 ± 20 µm, as determined by SEM) renders impossible direct visualization, reason why a thinner membrane section was previously prepared by cryo-microtomy (cf. Section 2.4). The TEM micrographs of the microtomed sample confirm the uniform distribution of rGO-M within the porous surface of the nanocomposite membrane (cf. Fig. 8h and i). The strong and sharp diffraction spots observed in the electron diffraction pattern of rGO-M-PVDF (cf. Fig. 8g) suggest the existence of oriented single PVDF crystals.

3.2. Activated persulfate oxidation in continuous mode

A non-catalytic experiment was performed in batch mode to evaluate the possible oxidation of the MPs by SPS alone. After 24 h, the conversion of OFX, CIP and EFX was negligible, i.e., below 5%. Experiments were then performed in continuous mode, in order to evaluate the performance of the metal-free carbon-based polymer nanocomposite membranes (rGO-M-PVDF) against that of supported membranes prepared by simple vacuum filtration of rGO-M into a PTFE substrate. This comparison was performed under constant flow conditions [37].

First, a pure adsorption run was performed with the rGO-M supported membrane (cf. Fig. 9a). As observed, a sharp decrease is observed at the beginning of the adsorption process, the membrane

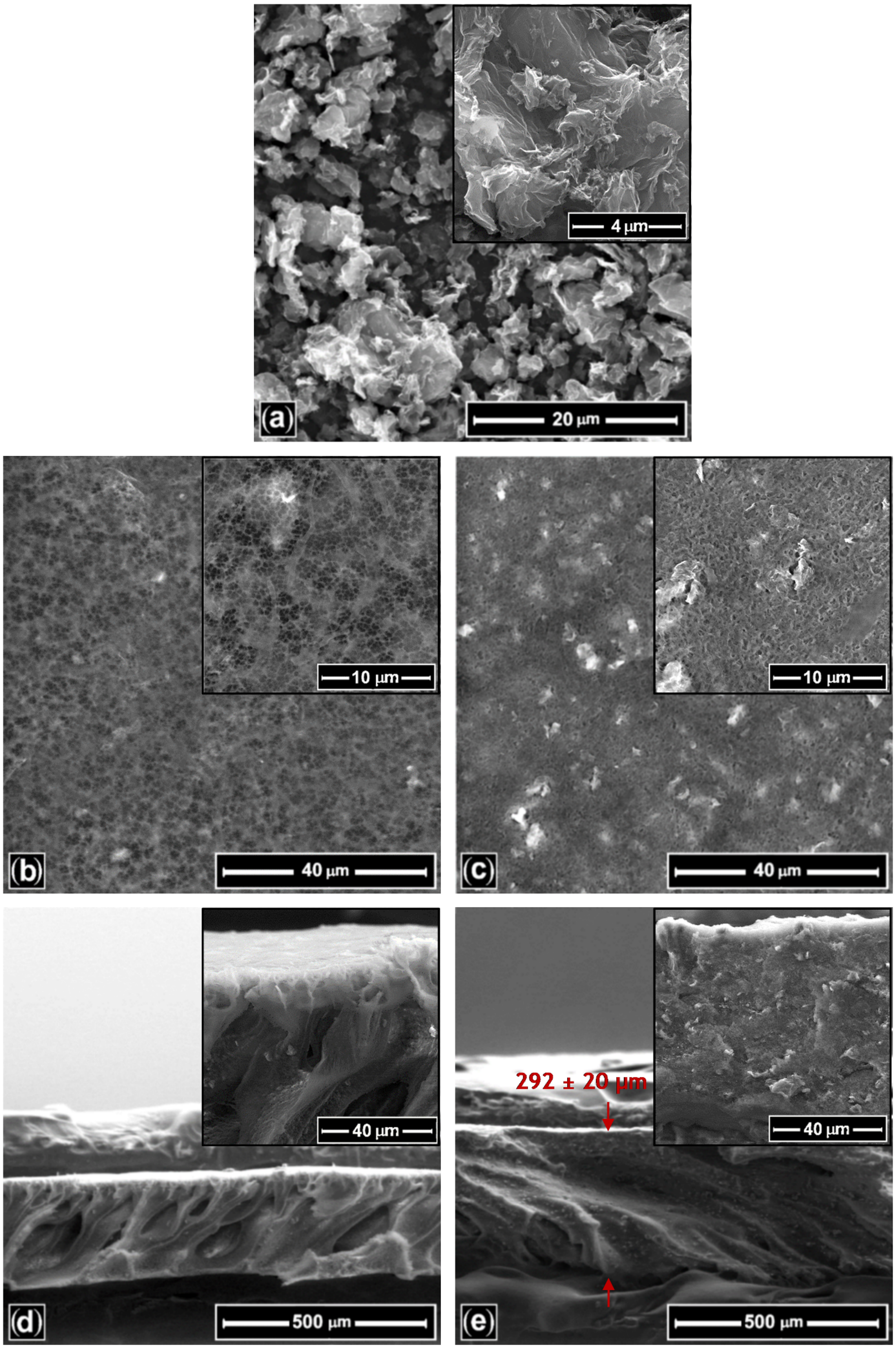

Fig. 5. SEM micrographs of (a) rGO-M in powder form, and (b, d) PVDF and (c, e) rGO-M-PVDF membranes. (b, c) top and (d, e) cross-sectional views.

becoming increasingly saturated until reaching negligible adsorption at the end of the experiment. In contrast, the degradation of the three target antibiotics increases significantly when SPS is added (cf. Fig. 9b). Specifically, removals in the range 85 – 90% are obtained for the three MPs, corresponding to average pollutant mass removal rates in the range 2.56 – 2.72 mg m^{-2} h^{-1} (determined as described in Eq. (4), and detailed in Table S4 and Fig. S6). It was concluded, in our previous study, that this effect can be ascribed to the presence of nitrogen species on the surface of rGO-M, in particular N-pyridinic groups, which account for a catalytic mechanism including radical and non-radical (mainly singlet oxygen species) oxidation pathways during the degradation of phenol and oxalic acid [14]. Briefly, these mechanistic insights were obtained as follows: (i) selective radical scavengers (methanol as scavenger of $SO_4^{\bullet-}$ and $HO^{\bullet}$ radicals, and furfuryl alcohol as scavenger of singlet oxygen) were employed, the results revealing that the catalytic mechanism is governed both by radical and non-radical oxidation pathways, although a more pronounced contribution of singlet oxygen was observed; and (ii) XPS was used to characterize pristine and used membranes, which allowed correlating the loss of N-pyridinic groups with the partial loss of catalytic activity during the reaction, thus suggesting that these surface groups are the main active sites involved in the catalytic process – in the opposite, N-pyrrolic and N-quaternary groups remained in the used membrane [14].

The adsorption behaviour when rGO-M-PVDF nanocomposite membranes are employed (Fig. 10a) is similar to that obtained with

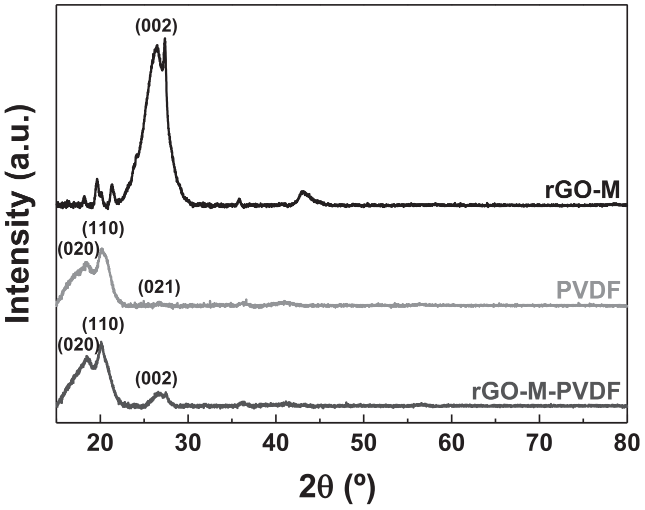

Fig. 6. XRD diffraction patterns of rGO-M in powder form, and PVDF and rGO-M-PVDF membranes.

supported membranes (Fig. 9a). Once again, the adsorption of the three MPs under study is negligible after 24 h of operation in continuous mode (Fig. 10a). When SPS is added (Fig. 10b), the removal of the target MPs obtained after 24 h increases up to 54, 77 and 91%, for OFX, CIP and EFX, respectively. After the sharp decrease observed at the beginning of the oxidation process, the removal of OFX decreases from 80% after 1 h, to 54% after 24 h, while the removals of CIP and EFX are less affected during the same period. In this case, the average pollutant mass removal rates obtained during the 24 h experiments are in the range 2.05 – 2.73 mg m^{-2} h^{-1} (cf. Table S4 and Fig. S6). These results show for the first time that metal-free carbon-based polymer nanocomposite membranes are effective for the degradation of MPs by activated persulfate oxidation in continuous mode of operation.

SPS consumption, monitored during activated persulfate experiments, revealed that both membranes are able to promote the decomposition of SPS (cf. Fig. 9b and 10b). Moreover, the low amount of SPS employed (25 mg L^{-1}) corresponds to a maximum of 10.1 mg L^{-1} of sulphates in the treated water, which is ca. 25-fold lower even than the current drinking water standards established in the EU Drinking Water Directive [38]. Water permeate flux (J_W) was also monitored. Although polymeric membranes are less hydrophilic (c.f. Section 3.1), J_W is approximately the same during the experiments performed with the two types of membranes. Moreover, fouling was apparently negligible for both membranes, as concluded from nearly constant J_W values. This observation can be ascribed to the antifouling properties of graphene-based materials [21].

The performance of the rGO-M-PVDF nanocomposite membranes for activated persulfate oxidation is still worse than that obtained with rGO-M supported membranes prepared by simple filtration into a PTFE substrate. This can be explained by the lower amount of the active rGO-M material found in each membrane. While supported membranes possess 15 mg of rGO-M (i.e. 100 wt% of rGO-M layer on the PTFE support), rGO-M-PVDF membranes possess only 6.4 wt% of rGO-M corresponding to ca. 1.5 mg (i.e. a much lower amount of catalytic active phase). Moreover, it should be noted that rGO-M-PVDF nanocomposite polymeric membranes have considerable advantages regarding possible future industrial applications. These membranes are structurally stable under the operating conditions considered in this study, maintaining their shape, while supported membranes undergo partial disintegration more easily upon continuous operation, drying and/or reuse. Moreover, the mass fraction of rGO-M included in rGO-M-PVDF nanocomposite membranes can be the object of further optimization when treating pollutants in realistic matrices, now that the catalytic activity of these polymer membranes for activated persulfate oxidation in continuous mode has been shown.

Having this ultimate goal in mind, preliminary experiments were performed with SW instead of UP water (cf. Fig. S7). As observed, the efficiency of the treatment process decreases when using both rGO-M supported (cf. Fig. S7b) and rGO-M-PVDF (cf. Fig. S7d) membranes. Specifically, the average pollutant mass removal rates obtained during the 24 h activated persulfate oxidation experiments are in the range 0.52 – 1.33 mg m^{-2} h^{-1} and 0.34 – 0.77 mg m^{-2} h^{-1}, for supported and rGO-M-PVDF nanocomposite membranes, respectively (cf. Table S4). Less consumption of SPS is also observed under these conditions, when compared to that obtained with the UP water matrix. Several studies report that the efficiency of the treatment processes can decrease considerably when real water matrices are used instead of simulated ones [1,39]. Our results confirm this trend. The lower conversion of SPS observed in SW suggests that less radical and non-radical active species may be formed due to presence of many ions and/or natural organic matter (cf. Section 2.2), thus affecting the performance of the treatment. Since many factors can dictate the efficiency of activated persulfate oxidation [40,41], additional experiments are needed to understand the effect of water environmental factors. Likewise, more studies on the optimization of both membrane design and operating conditions are also needed. These experiments should be performed under realistic conditions.

3.3. Literature survey on carbon-based membranes for activated persulfate oxidation

The literature reporting the application of metal containing and metal-free carbon-based membranes for activated persulfate oxidation is summarized in Tables S5 and S6, respectively. The first conclusion to be withdrawn is that this is a very recent research topic, since all the

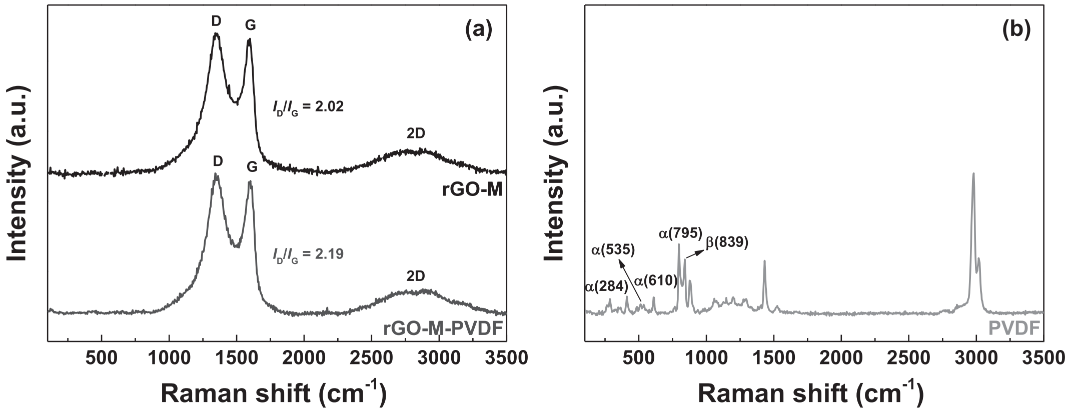

Fig. 7. Raman spectra of (a) rGO-M in powder form and rGO-M-PVDF membrane, and (b) PVDF membrane.

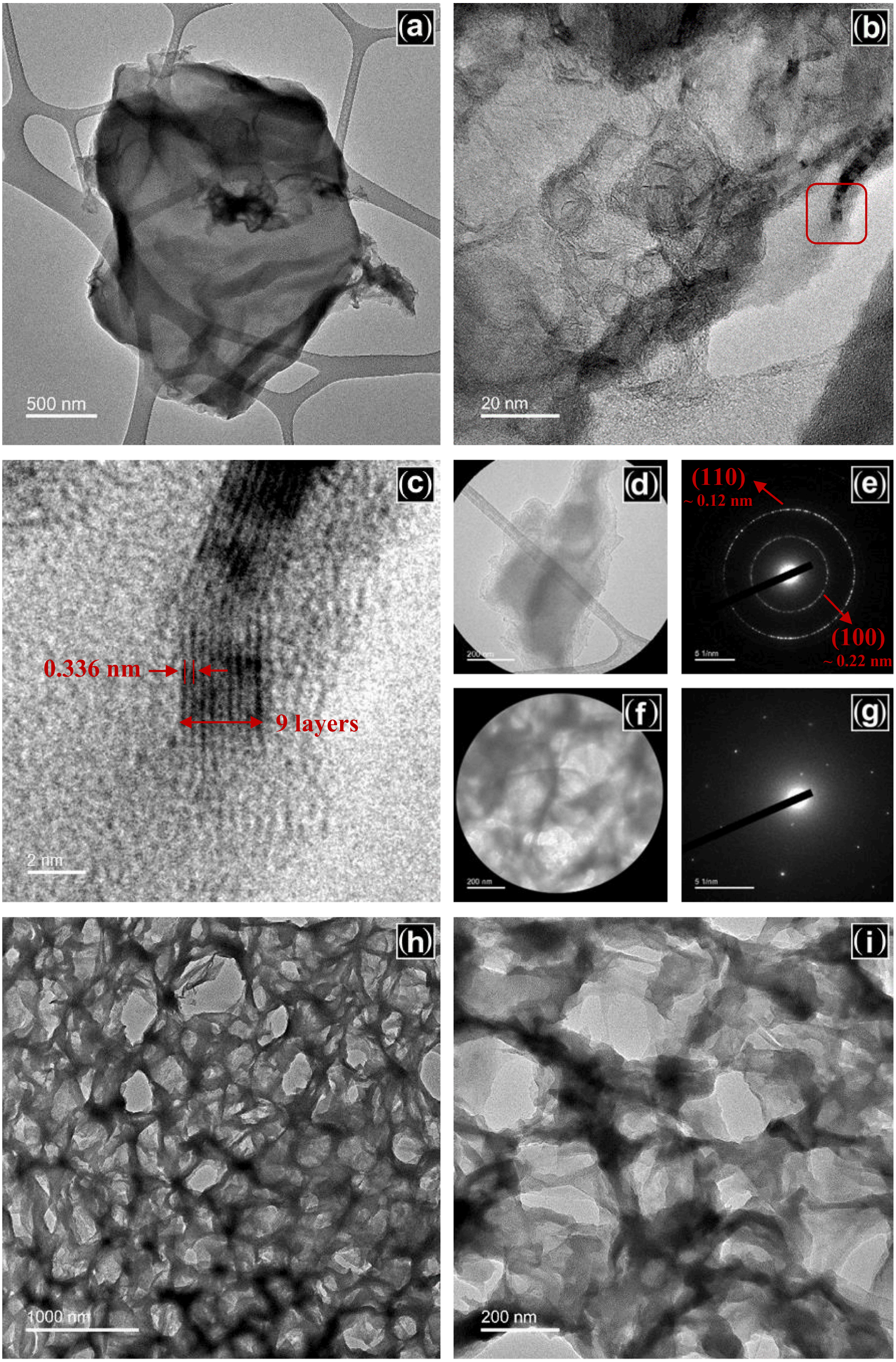

(caption on next page)

Fig. 8. TEM micrographs of (a, b, c, d) rGO-M in powder form and (f, h, i) rGO-M-PVDF membrane. The image in (c) is a magnification of the section identified by a red box in (b). Electron diffraction patterns of (e) rGO-M and (g) rGO-M-PVDF, collected in the sections given in (d) and (f), respectively. (For interpretation of the references to color in this figure legend, the reader is referred to the web version of this article.)

nine articles have been published since 2016 (including four in 2019, and three already in 2020). Secondary contamination due to metal leaching occurs when using metal containing membranes (cf. Table S5) – including with priority metals in the field of water policy such as nickel (as defined in Directive 2013/39/EU), and therefore has to be taken into account when selecting catalysts for persulfate oxidation of organic pollutants.

Only one out of the six studies reported on the application of metal containing carbon-based membranes was performed in continuous mode (cf. Table S5) [42]; the other five studies were performed in batch or semi-continuous (under recirculation) mode [43–47]. On the contrary, all the three studies reported on the application of metal-free carbon-based membranes were performed in continuous mode (cf. Table S6) [13–15]. Nevertheless, the membranes used in these three studies were obtained by simple vacuum filtration of the catalytic active phase into a PTFE [13,14] or nylon [15] support. Likewise, vacuum filtration is the technique most commonly employed to fabricate metal containing membranes for activated persulfate oxidation [44,46,47], followed by incorporation of the metal-based catalytic active phase in a PVDF matrix by mixing in the membrane forming materials [43], dip-coating [42] and sol-gel electrospinning [45]. In the only study previously reported on the application of a carbon–PVDF composite membrane for activated persulfate oxidation – performed by Yao et al. [43], a metal containing carbon material, obtained by thermal annealing of dicyandiamide, thiourea and iron (III), was employed as active phase. Moreover, the resulting composite membrane was only employed in experiments performed in batch mode. It is thus confirmed that the present study reports for the first time the use of metal-free carbon-based polymer nanocomposite membranes for activated persulfate oxidation in continuous mode of operation. Moreover, this study is performed under more realistic conditions (i.e., simultaneous degradation of three fluoroquinolone antibiotics at 100 μg L^{-1} each), and during a longer period of time (24 h) than the other studies previously reported (in the range 2.5 – 6.5 h). Indeed, this is also the first study reporting the application of a carbon-based catalytic membrane in activated persulfate oxidation experiments performed in continuous mode with a real water matrix (i.e., SW). Moreover, none of the studies under

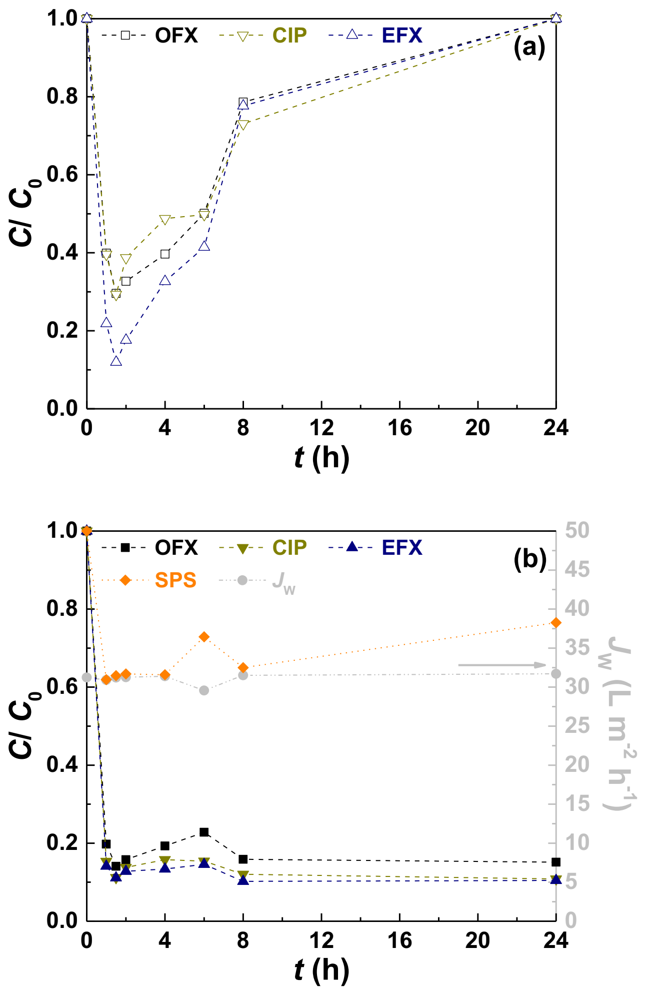

Fig. 9. Removal of OFX, CIP and EFX obtained in (a) adsorption, and (b) activated persulfate oxidation experiments performed in UP water, with rGO-M supported membranes. Water permeate flux (J_w) and conversion of SPS are also shown in (b). Experiments performed with $[OFX]_0$ = $[CIP]_0$ = $[EFX]_0$ = 100 μg L^{-1}, $[SPS]_0$ = 25 mg L^{-1}, pH$_0$ = 5.9 (inherent pH), Q = 0.1 mL min^{-1} (continuous mode), and T = 22 ± 2 °C.

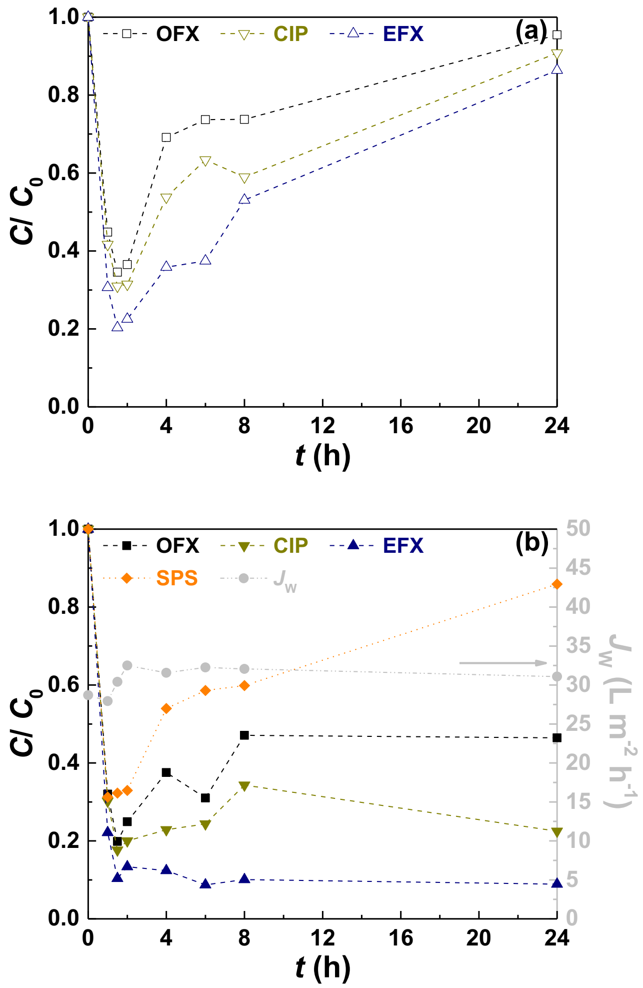

Fig. 10. Removal of OFX, CIP and EFX obtained in (a) adsorption, and (b) activated persulfate oxidation experiments performed in UP water, with rGO-M-PVDF membranes. Water permeate flux (J_w) and conversion of SPS are also shown in (b). Experiments performed under the conditions given in Fig. 9.

discussion follows nor oxidant consumption (persulfate or peroxymonosulfate), nor water permeate flux during the experiments performed in continuous mode. On the contrary, all these data are provided in this study.

4. Conclusions

Metal-free carbon-based polymer nanocomposite membranes (rGO-M-PVDF) are effective for activated persulfate oxidation in continuous mode of operation for the simultaneous degradation of three fluoroquinolone antibiotics at realistic concentrations (100 $\mu g\,L^{-1}$ each). Conversions in the range 54 – 91% were achieved after 24 h of continuous operation. Moreover, the effectiveness of rGO-M-PVDF for the conversion of persulfate was demonstrated, and water permeate flux measurements revealed the high resistance of these nanocomposite membranes towards fouling phenomena. Nevertheless, the performance of the treatment process decreased in preliminary experiments performed with surface water instead of ultrapure water. Additional studies are thus needed to overcome this detrimental effect.

Declaration of Competing Interest

The authors declare that they have no known competing financial interests or personal relationships that could have appeared to influence the work reported in this paper.

Acknowledgments

This work was financially supported by project NORTE-01-0145-FEDER-031049 (InSpeCt -PTDC/EAM-AMB/31049/2017) funded by FEDER funds through NORTE 2020 – Programa Operacional Regional do NORTE, and by national funds (PIDDAC) through FCT/MCTES. We would also like to thank the scientific collaboration under Base Funding – UIDP/50020/2020 of the Associate Laboratory LSRE-LCM – funded by national funds through FCT/MCTES (PIDDAC). Technical assistance with SEM analysis is gratefully acknowledged to CEMUP team. Technical assistance with TEM, XRD and Raman analysis is gratefully acknowledged to INL.

Appendix A. Supplementary data

Supplementary data to this article can be found online at https://doi.org/10.1016/j.cej.2020.126117.

References

[1] M.O. Barbosa, N.F.F. Moreira, A.R. Lado Ribeiro, M.F.R. Pereira, A.M.T. Silva, Occurrence and removal of organic micropollutants: an overview of the watch list of EU Decision 2015/495, Water Res. 94 (2016) 257–279, https://doi.org/10.1016/j.watres.2016.02.047.

[2] A.R. Lado Ribeiro, O.C. Nunes, M.F.R. Pereira, A.M.T. Silva, An overview on the advanced oxidation processes applied for the treatment of water pollutants defined in the recently launched Directive 2013/39/EU, Environ. Int. 75 (2015) 33–51, https://doi.org/10.1016/j.envint.2014.10.027.

[3] J. Wang, S. Wang, Activation of persulfate (PS) and peroxymonosulfate (PMS) and application for the degradation of emerging contaminants, Chem. Eng. J. 334 (2018) 1502–1517, https://doi.org/10.1016/j.cej.2017.11.059.

[4] J.C.G. Sousa, A.R. Lado Ribeiro, M.O. Barbosa, M.F.R. Pereira, A.M.T. Silva, A review on environmental monitoring of water organic pollutants identified by EU guidelines, J. Hazard. Mater. 344 (2018) 146-162. doi: 10.1016/j.jhazmat.2017.09.058.

[5] L. Rizzo, S. Malato, D. Antakyali, V.G. Beretsou, M.B. Đolić, W. Gernjak, E. Heath, I. Ivancev-Tumbas, P. Karaolia, A.R. Lado Ribeiro, G. Mascolo, C.S. McArdell, H. Schaar, A.M.T. Silva, D. Fatta-Kassinos, Consolidated vs new advanced treatment methods for the removal of contaminants of emerging concern from urban wastewater, Sci. Total Environ. 655 (2019) 986–1008, https://doi.org/10.1016/j.scitotenv.2018.11.265.

[6] Q. Zhao, Q. Mao, Y. Zhou, J. Wei, X. Liu, J. Yang, L. Luo, J. Zhang, H. Chen, H. Chen, L. Tang, Metal-free carbon materials-catalyzed sulfate radical-based advanced oxidation processes: a review on heterogeneous catalysts and applications, Chemosphere 189 (2017) 224–238, https://doi.org/10.1016/j.chemosphere.2017.09.042.

[7] X. Duan, H. Sun, S. Wang, Metal-free carbocatalysis in advanced oxidation reactions, Acc. Chem. Res. 51 (2018) 678–687, https://doi.org/10.1021/acs.accounts.7b00535.

[8] R. Xiao, Z. Luo, Z. Wei, S. Luo, R. Spinney, W. Yang, D.D. Dionysiou, Activation of peroxymonosulfate/persulfate by nanomaterials for sulfate radical-based advanced oxidation technologies, Curr. Opin. Chem. Eng. 19 (2018) 51–58, https://doi.org/10.1016/j.coche.2017.12.005.

[9] E. Doustkhah, Y. Ide, Microporous layered silicates: old but new microporous materials, New J. Chem. (2020), https://doi.org/10.1039/C9NJ06222J.

[10] J.L. Figueiredo, Functionalization of porous carbons for catalytic applications, J. Mater. Chem. A 1 (2013) 9351–9364, https://doi.org/10.1039/C3TA10876G.

[11] P. Serp, M. Corrias, P. Kalck, Carbon nanotubes and nanofibers in catalysis, Appl. Catal. A 253 (2003) 337–358, https://doi.org/10.1016/S0926-860X(03)00549-0.

[12] P. Serp, J.L. Figueiredo, Carbon materials for catalysis, John Wiley & Sons, Inc., Hoboken, New Jersey, 2009.

[13] Y. Liu, L. Yu, C.N. Ong, J. Xie, Nitrogen-doped graphene nanosheets as reactive water purification membranes, Nano Res. 9 (2016) 1983–1993, https://doi.org/10.1007/s12274-016-1089-7.

[14] M. Pedrosa, G. Drazic, P.B. Tavares, J.L. Figueiredo, A.M.T. Silva, Metal-free graphene-based catalytic membrane for degradation of organic contaminants by persulfate activation, Chem. Eng. J. 369 (2019) 223–232, https://doi.org/10.1016/j.cej.2019.02.211.

[15] J. Sheng, H. Yin, F. Qian, H. Huang, S. Gao, J. Wang, Reduced graphene oxide-based composite membranes for in-situ catalytic oxidation of sulfamethoxazole operated in membrane filtration, Sep. Purif. Technol. 236 (2020) 116275, https://doi.org/10.1016/j.seppur.2019.116275.

[16] F. Liu, N.A. Hashim, Y. Liu, M.R.M. Abed, K. Li, Progress in the production and modification of PVDF membranes, J. Membr. Sci. 375 (2011) 1–27, https://doi.org/10.1016/j.memsci.2011.03.014.

[17] M.O. Barbosa, A.R. Lado Ribeiro, N. Ratola, E. Hain, V. Homem, M.F.R. Pereira, L. Blaney, A.M.T. Silva, Spatial and seasonal occurrence of micropollutants in four Portuguese rivers and a case study for fluorescence excitation-emission matrices, Sci. Total Environ. 644 (2018) 1128–1140, https://doi.org/10.1016/j.scitotenv.2018.06.355.

[18] Commission Implementing Decision (EU) 2018/840 of 5 June 2018 establishing a watch list of substances for Union-wide monitoring in the field of water policy pursuant to Directive 2008/105/EC of the European Parliament and of the Council and repealing Commission Implementing Decision (EU) 2015/495, in, Official Journal of the European Union, 2018.

[19] M. Pedrosa, L.M. Pastrana-Martínez, M.F.R. Pereira, J.L. Faria, J.L. Figueiredo, A.M.T. Silva, N/S-doped graphene derivatives and TiO_2 for catalytic ozonation and photocatalysis of water pollutants, Chem. Eng. J. 348 (2018) 888–897, https://doi.org/10.1016/j.cej.2018.04.214.

[20] D. Li, X. Duan, H. Sun, J. Kang, H. Zhang, M.O. Tade, S. Wang, Facile synthesis of nitrogen-doped graphene via low-temperature pyrolysis: the effects of precursors and annealing ambience on metal-free catalytic oxidation, Carbon 115 (2017) 649–658, https://doi.org/10.1016/j.carbon.2017.01.058.

[21] S. Ayyaru, Y.-H. Ahn, Application of sulfonic acid group functionalized graphene oxide to improve hydrophilicity, permeability, and antifouling of PVDF nanocomposite ultrafiltration membranes, J. Membr. Sci. 525 (2017) 210–219, https://doi.org/10.1016/j.memsci.2016.10.048.

[22] J.L. Figueiredo, M.F.R. Pereira, M.M.A. Freitas, J.J.M. Órfão, Modification of the surface chemistry of activated carbons, Carbon 37 (1999) 1379–1389, https://doi.org/10.1016/S0008-6223(98)00333-9.

[23] J.L. Figueiredo, M.F.R. Pereira, M.M.A. Freitas, J.J.M. Órfão, Characterization of active sites on carbon catalysts, Ind. Eng. Chem. Res. 46 (2007) 4110–4115, https://doi.org/10.1021/ie061071v.

[24] Y. Yuan, T.R. Lee, Contact angle and wetting properties, in: Surface science techniques, G. Bracco, B. Holst Springer Berlin Heidelberg, Berlin, 2013, pp. 3-34.

[25] S. Gokulakrishnan, A. Mohammed, H. Prakash, Determination of persulphates using N, N-diethyl-p-phenylenediamine as colorimetric reagent: oxidative coloration and degradation of the reagent without bactericidal effect in water, Chem. Eng. J. 286 (2016) 223–231, https://doi.org/10.1016/j.cej.2015.10.058.

[26] A.M. Gorito, A.R. Lado Ribeiro, C.R. Gomes, C.M.R. Almeida, A.M.T. Silva, Constructed wetland microcosms for the removal of organic micropollutants from freshwater aquaculture effluents, Sci. Total Environ. 644 (2018) 1171–1180, https://doi.org/10.1016/j.scitotenv.2018.06.371.

[27] 2540 Solids, in: Standard Methods for the Examination of Water and Wastewater, E. W. Rice, R.B. Baird, A.D. Eaton American Public Health Association, American Water Works Association, Water Environment Federation, 2017.

[28] X. Zhao, J. Ma, Z. Wang, G. Wen, J. Jiang, F. Shi, L. Sheng, Hyperbranched-polymer functionalized multi-walled carbon nanotubes for poly (vinylidene fluoride) membranes: from dispersion to blended fouling-control membrane, Desalination 303 (2012) 29–38, https://doi.org/10.1016/j.desal.2012.07.009.

[29] B.F. Machado, P. Serp, Graphene-based materials for catalysis, Catal. Sci. Technol. 2 (2011) 54–75, https://doi.org/10.1039/C1CY00361E.

[30] X. Jiao, Y. Qiu, L. Zhang, X. Zhang, Comparison of the characteristic properties of reduced graphene oxides synthesized from natural graphites with different graphitization degrees, RSC Adv. 7 (2017) 52337–52344, https://doi.org/10.1039/C7RA10809E.

[31] X. Cai, T. Lei, D. Sun, L. Lin, A critical analysis of the α, β and γ phases in poly (vinylidene fluoride) using FTIR, RSC Adv. 7 (2017) 15382–15389, https://doi.org/10.1039/C7RA01267E.

[32] M.S. Dresselhaus, A. Jorio, M. Hofmann, G. Dresselhaus, R. Saito, Perspectives on carbon nanotubes and graphene raman spectroscopy, Nano Lett. 10 (2010)

751–758, https://doi.org/10.1021/nl904286r.

[33] R.S. Ribeiro, A.M.T. Silva, L.M. Pastrana-Martínez, J.L. Figueiredo, J.L. Faria, H.T. Gomes, Graphene-based materials for the catalytic wet peroxide oxidation of highly concentrated 4-nitrophenol solutions, Catal. Today 249 (2015) 204–212, https://doi.org/10.1016/j.cattod.2014.10.004.

[34] F. Xu, K. Zhang, Y. Zhou, Z. Qu, H. Wang, Y. Zhang, H. Zhou, C. Yan, Facile preparation of highly oriented poly(vinylidene fluoride) uniform films and their ferro- and piezoelectric properties, RSC Adv. 7 (2017) 17038–17043, https://doi.org/10.1039/C7RA00586E.

[35] N.R. Wilson, P.A. Pandey, R. Beanland, R.J. Young, I.A. Kinloch, L. Gong, Z. Liu, K. Suenaga, J.P. Rourke, S.J. York, J. Sloan, Graphene oxide: structural analysis and application as a highly transparent support for electron microscopy, ACS Nano 3 (2009) 2547–2556, https://doi.org/10.1021/nn900694t.

[36] A. Bianco, H.-M. Cheng, T. Enoki, Y. Gogotsi, R.H. Hurt, N. Koratkar, T. Kyotani, M. Monthioux, C.R. Park, J.M.D. Tascon, J. Zhang, All in the graphene family – a recommended nomenclature for two-dimensional carbon materials, Carbon 65 (2013) 1–6, https://doi.org/10.1016/j.carbon.2013.08.038.

[37] D.J. Miller, S. Kasemset, D.R. Paul, B.D. Freeman, Comparison of membrane fouling at constant flux and constant transmembrane pressure conditions, J. Membr. Sci. 454 (2014) 505–515, https://doi.org/10.1016/j.memsci.2013.12.027.

[38] Council Directive 98/83/EC of 3 November 1998 on the quality of water intended for human consumption, in, Official Journal of the European Communities, The Council of the European Union, 1998.

[39] A.R. Lado Ribeiro, N.F.F. Moreira, G. Li Puma, A.M.T. Silva, Impact of water matrix on the removal of micropollutants by advanced oxidation technologies, Chem. Eng. J. 363 (2019) 155–173, https://doi.org/10.1016/j.cej.2019.01.080.

[40] R.S. Ribeiro, Z. Frontistis, D. Mantzavinos, A.M.T. Silva, J.L. Faria, H.T. Gomes, Screening of heterogeneous catalysts for the activated persulfate oxidation of sulfamethoxazole in aqueous matrices. Does the matrix affect the selection of catalyst? J. Chem. Technol. Biotechnol. 94 (2019) 2425–2432, https://doi.org/10.1002/jctb.6080.

[41] M.E. Metheniti, Z. Frontistis, R.S. Ribeiro, A.M.T. Silva, J.L. Faria, H.T. Gomes, D. Mantzavinos, Degradation of propyl paraben by activated persulfate using iron-containing magnetic carbon xerogels: investigation of water matrix and process synergy effects, Environ. Sci. Pollut. Res. 25 (2018) 34801–34810, https://doi.org/10.1007/s11356-017-0178-9.

[42] Y. Bao, Y.S. Tay, T.-T. Lim, R. Wang, R.D. Webster, X. Hu, Polyacrylonitrile (PAN)-induced carbon membrane with in-situ encapsulated cobalt crystal for hybrid peroxymonosulfate oxidation-filtration process: Preparation, characterization and performance evaluation, Chem. Eng. J. 373 (2019) 425–436, https://doi.org/10.1016/j.cej.2019.05.058.

[43] Y. Yao, C. Lian, Y. Hu, J. Zhang, M. Gao, Y. Zhang, S. Wang, Heteroatoms doped metal iron–polyvinylidene fluoride (PVDF) membrane for enhancing oxidation of organic contaminants, J. Hazard. Mater. 338 (2017) 265–275, https://doi.org/10.1016/j.jhazmat.2017.05.026.

[44] J. Kang, H. Zhang, X. Duan, H. Sun, X. Tan, S. Liu, S. Wang, Magnetic Ni-Co alloy encapsulated N-doped carbon nanotubes for catalytic membrane degradation of emerging contaminants, Chem. Eng. J. 362 (2019) 251–261, https://doi.org/10.1016/j.cej.2019.01.035.

[45] H. Shan, X. Dong, X. Cheng, Y. Si, J. Yu, B. Ding, Highly flexible, mesoporous structured, and metallic Cu-doped C/SiO_2 nanofibrous membranes for efficient catalytic oxidative elimination of antibiotic pollutants, Nanoscale 11 (2019) 14844–14856, https://doi.org/10.1039/C9NR04118D.

[46] Z. Wang, L.-C. Nengzi, X. Zhang, Z. Zhao, X. Cheng, Novel $NiCo_2S_4$/CS membranes as efficient catalysts for activating persulfate and its high activity for degradation of nimesulide, Chem. Eng. J. 381 (2020) 122517, https://doi.org/10.1016/j.cej.2019.122517.

[47] C. Chen, M. Xie, L. Kong, W. Lu, Z. Feng, J. Zhan, Mn_3O_4 nanodots loaded g-C_3N_4 nanosheets for catalytic membrane degradation of organic contaminants, J. Hazard. Mater. 390 (2020) 122146, https://doi.org/10.1016/j.jhazmat.2020.122146.